Therapeutic efficacy of in-vivo IL-12 plasmid delivery using microbubble-assisted ultrasound in a B16F10 mouse melanoma model: A proof of concept

Edward Oujagir, Coralie Mousset, Marie Roy, Yanis Ramdani, Valérie Schubnel, Chloé Boisseau, Sylviane Marouillat, Rose-Anne Thépault, Damien Fouan, Jean-Yves Tartu, et al.

Therapeutic efficacy of *in-vivo* IL-12 plasmid delivery using microbubble-assisted ultrasound in a B16F10 mouse melanoma model: A proof of concept

Edward Oujagir[1,2¶], Coralie Mousset[1¶], Marie Roy[1¶], Yanis Ramdani[2], Valérie Schubnel[1], Chloé Boisseau[1], Sylviane Marouillat[1], Rose-Anne Thépault[3], Damien Fouan[1], Jean-Yves Tartu[1], Ayache Bouakaz[1], Sophie Serrière[1], Valérie Gouilleux-Gruart[2], Jean-Michel Escoffre[1]*

[1]Université de Tours, INSERM, Imaging Brain & Neuropsychiatry iBraiN U1253, 37032, Tours, France

[2] Present address: Université de Tours, INSERM, CEPR U1100, 37032 Tours, France

[3]Present address: Université d'Angers, Nantes Université, CNRS, INSERM, Centre de Recherche en Cancérologie et Immunologie Intégrée Nantes Angers CRCI2NA U1307, 44007, Nantes, France

AUTHOR INFORMATION

Author contributions:

[¶]E. Oujagir, C. Mousset & M. Roy contributed equally to this work.

Corresponding Author

J-M. Escoffre, PhD., Inserm UMR 1253, Université de Tours, 10 bd Tonnellé, 37032 Tours Cedex, France. Tel. +33 (0) 247366191. Email: jean-michel.escoffre@univ-tours.fr.

HIGHLIGHTS

- MB-assisted US enables efficient intratumoral pIL-12 delivery
- Local pIL-12 expression activates NK cells and boosts antitumor immunity
- Acoustically mediated pIL-12 delivery significantly reduces melanoma growth
- This approach improves mouse health compared with pIL-12 injection alone

ABSTRACT

In-vivo targeted delivery of immunostimulatory molecules for melanoma treatment is a promising strategy to overcome complexity, toxicity, and cost associated with current immunotherapies. Among these molecules, interleukine-12 (IL-12) is a potent immunostimulatory cytokine that plays a major role in antitumoral immune response. However, systemic administration of IL-12 induces severe side effects, highlighting the need for efficient and safe *in-vivo* delivery modalities. Microbubble-assisted ultrasound (MB-assisted US) is an emerging non-invasive and targeted method for therapeutic molecule delivery. This study aimed to evaluate its efficacy for intratumoral (i.t.) delivery of a plasmid encoding IL-12 (pIL-12) in a mouse melanoma model. *In-vitro*, delivery of 5 or 10 μg of pIL-12 into melanoma cell suspensions using MB-assisted US increased IL-12 concentration to 1429 ± 125 and 2352 ± 125 pg/mL, respectively, whereas pIL-12 treatment alone did not elicit IL-12 secretion. Similarly, acoustically mediated delivery of 10 or 50 μg of pIL-12 into melanoma spheroids significantly increased IL-12 concentration - 131 ± 7 and 250 ± 60 pg/mL respectively - compared to pIL-12 alone (0 pg/mL for 10 μg and 7.5 ± 7.5 pg/mL for 50 μg). *In-vivo,* acoustically mediated pIL-12 delivery increased serum mIL-12 concentration by 5-fold compared with i.t. pIL-12 injection alone, promoting NK cell recruitment and activation within the tumor microenvironment. By day 15, this strategy reduced tumor volume by 2.5-fold relative to i.t. pIL-12 alone and improved mouse health status. These findings confirm that MB-assisted US is a relevant modality for *in-vivo* delivery of immunostimulatory molecules in melanoma therapy.

KEYWORDS: Melanoma - interleukin-12 – microbubbles – ultrasound – sonoporation - immunotherapy

1. Introduction

In Europe, malignant melanoma (MM) is a rare skin cancer and among the most aggressive and lethal variants. However, its incidence has been increasing [1]. In 2020, the estimated number of new MM cases and related deaths for both sexes were 150,600 and 26,400, respectively [2]. Nowadays, the average cost for MM diagnosis and treatment is 10 times greater than that of other skin malignancies [3]. At early stages (*i.e.,* localized stage or stages I and II), MM is curable with surgery, with a 5-year specific survival rate of 98% [4]. However, worse outcomes have been observed for patients with late-stage melanoma. For example, the 5-y specific survival rate of patients with late-stage melanoma undergoing conventional therapies, including chemotherapy and radiotherapy, is only 5% [4]. Notably, new yet costly biologic and/or targeted therapies (*e.g.,* dendritic cell vaccines, therapeutic antibodies, and checkpoint, BRAF, and MEK inhibitors) have been developed and validated for the treatment of advanced MM stages, increasing the 5-y survival rate to 50% [5]. Among these therapies, dendritic cell (DC) vaccines have emerged as a promising therapeutic strategy in recent years [6]. For instance, DC vaccination induced an objective clinical response in 10% of patients with stage III/IV melanoma, a rate comparable to that achieved with ipilimumab-based immunotherapy [7]. Moreover, Wilgenhof *et al.,* reported that DC vaccination resulted in durable responses in more than 25% of patients with stage III/IV melanoma [8]. However, this process is complex and expensive, limiting its broader use. The main reason is that these vaccines are generated *ex-vivo* from autologous DCs, tailored for each patient.

Notably, *in-vivo* delivery of immunostimulatory molecules (*i.e.,* tumor antigens and cytokines) could circumvent the laborious and costly procedures involved in the design of DC vaccines. Among these molecules, interleukin 12 (IL-12) is a very attractive cytokine due to its ability to activate both adaptive and innate immune systems [9]. IL-12 is mainly produced by DCs, macrophages, and certain B lymphocyte subsets. It plays a central role in driving the

differentiation of naïve T lymphocytes into type 1 helper CD4 T lymphocytes (Th1) and enhancing the cytotoxic activities of cytotoxic T lymphocytes (CTLs), CD8 T lymphocytes, and natural killer (NK) cells [9]. IL-12 is also involved in the anti-angiogenic activities of the CXCL-10 chemokine by stimulating interferon γ (IFN-γ) production. In addition, IL-12 exerts positive feedback on its own secretion: IL-12-induced IFN-γ secretion by Th1 and CTLs acts on DCs to enhance IL-12 production. These functions highlight IL-12 as a key cytokine that boosts the anti-tumor immune response. Notably, some clinical studies have reported that systemic administration of recombinant IL-12 causes serious side effects in patients with advanced MM, whereas local administration reduced these side effects while maintaining therapeutic efficacy [10, 11]. Other preclinical and clinical studies advocate the *in-vivo* delivery of an IL-12-encoding plasmid (pIL-12) via electroporation (EP) [12-15]. Although this strategy achieved effective regression of primary and advanced MM, electroporation remains an invasive physical gene delivery method associated with local undesirable effects (*e.g.,* transient pain and muscle contraction) [16]. In addition, exposing tumor tissue to electric pulses requires positioning electrodes in direct contact with the treatment site, restricting its application to superficial tumors [17]. Consequently, this method requires invasive surgical procedures and/or the development of specialized electrodes [16, 17].

The design of a targeted, efficient, and safe gene delivery method remains a great challenge. Recently, microbubble-assisted ultrasound (MB-assisted US) has emerged as a promising physical modality for delivering therapeutic nucleic acids, including siRNA, microRNA, morpholino, mRNA and plasmid DNA (pDNA) [18]. These nucleic acids are injected *in-vivo* either in naked form or complexed with lipoplexes or polyplexes to protect them from enzymatic degradation [19]. Both formulations are administered with MBs *in-vivo*, either concurrently or sequentially. Nucleic acids can also be loaded onto the MB surface for co-delivery [19-21]. MBs and nucleic acids are typically administered either directly into the target

tissue or intravenously. The choice of nucleic acid formulations and the administration route for both agents depend largely on their physicochemical and pharmacological properties, as well as the desired therapeutic effect. The target tissue is generally exposed to US once the nucleic acids and the MBs have sufficiently accumulated into the target tissue or its microvasculature after intratissue or intravenous (i.v.) administration, respectively [19]. The acoustically triggered volumetric oscillations of MBs induce several local acoustic effects near the plasma membrane of target cells [22] or the endothelial wall of vessels [23] supplying the target tissue, which promote reversible permeabilization and facilitate transfection through the stimulation of intracellular, paracellular, and transcellular pathways [24]. This gene delivery modality offers several advantages inherent to US, including its ease of application, cost-effectiveness, safety, and clinical availability [24]. Moreover, US can penetrate the body and be directed to achieve targeted, non-invasive delivery of nucleic acids to superficial and deep-seated tissues, with minimal off-target effects, under US and magnetic resonance imaging guidance. A growing number of preclinical investigations have demonstrated the efficacy of MB-assisted US for delivery nucleic acids into the heart [25], skeletal muscle [26], liver [27], kidney [28], tumor [29, 30], brain [31, 32], pancreas [33], tendon [34], and vasculature [35, 36].

Recent preclinical investigations have explored the potential of MB-assisted US as a therapeutic modality for melanoma. This approach has been shown to enhance the intratumoral delivery and efficacy of various therapeutic agents, including chemotherapeutic drugs (*e.g.,* doxorubicin, paclitaxel) [37], photothermal agents (*e.g.,* gold nanorods, melanin nanoparticles) [38], and immunomodulatory molecules such as cytokines [39] and tumor-associated antigens [40, 41]. In murine melanoma models, MB-assisted US significantly improved i.t. drug accumulation, tumor growth inhibition, and overall survival, while reducing systemic toxicity [1]. Moreover, US guidance allows precise, localized, and repeatable treatments with minimal invasiveness. Despite these promising results, most studies have focused on small molecules or

nanoparticles, and few have addressed the acoustically mediated delivery of therapeutic pDNA in melanoma (for review [1]). Thus, the potential of MB-assisted US for the localized and non-invasive delivery of immunostimulatory pDNA, such as pIL-12, remains largely unexplored. Therefore, the present study addresses this gap by evaluating the efficiency and therapeutic efficacy of MB-assisted US–mediated intratumoral delivery of a plasmid encoding murine IL-12 (pIL-12) in a melanoma model. Building on this evidence, the present study aimed to evaluate the efficacy of the MB-assisted US for delivering a plasmid encoding murine IL-12 (pIL-12) *in-vitro* using melanoma cell suspensions and spheroids, as well as *in-vivo* using an aggressive murine melanoma model. This *in-vivo* model has also been exploited to investigate the anti-tumor efficacy of this strategy.

2. Materials and methods

2.1.Luciferase encoding plasmid (pLUC)

A 4.6-kpb plasmid, pLUC (pGL4.13[*luc2*/SV40] vector; Promega, Madison, WI, USA), encoding luciferase under the control of simian virus 40 promoter, was prepared from transformed Stellar™ competent cells (Clontech Laboratories, Inc., Mountain View, CA, USA) using the EndoFree® Plasmid purification system, following to the manufacturer's instructions (Qiagen, Hilden, Germany). The quantity and quality of pLUC were verified spectrophotometrically using a NanoDrop™ instrument (ThermoFisher Scientific, Waltham, MA, USA) and by agarose gel electrophoresis. Briefly, the UV absorbances of a 2 µL pLUC solution was measured at 230, 260, and 280 nm, with A260/A280 (range of 1.8-2.0) and A260/A230 (range of 2.0-2.2) ratios used as indicators of purity. The pLUC concentration was 2 µg/µL. Then, 2 µg of pLUC was mixed with 3 µL of 5X gel loading buffer (New England Biolabs® Inc., Ipswich, MA). This mixture, along with 1 µg of a 1 kbp DNA ladder (New England Biolabs® Inc.), was loaded onto a 0.8% agarose gel (Sigma-Aldrich, St. Louis, MO) prepared in 1X TBE buffer (100 mM Tris, 90 mM Borate, 1 mM EDTA and pH 8.3; Life

Technologies Corp., Carlsbad, CA) containing 0.05 ‰ ethidium bromide (Sigma-Aldrich). Electrophoresis was performed at 130 V for 45 min using a PowerPac power supply (Bio-Rad Laboratories B.V., Marne-La-Coquette, France), and the gel was visualized using a ChemiDoc™ XRS detection system (Bio-Rad Laboratories B.V.).

2.2.Interleukin-12 encoding plasmid (pIL-12)

A 4.6-kpb plasmid, pIL-12 (pCpGfree-mIL12; InvivoGen, San Diego, CA, USA), encoding murine interleukine-12 (mIL-12) (**Figure 1A**), was prepared from transformed *Escherichia coli* (GT115; InvivoGen) using the EndoFree® Plasmid purification system (Qiagen) [42]. As described above, the quantity and quality of pIL-12 (2 μg/μL) were verified using spectrophotometry and agarose gel electrophoresis. Restriction mapping of pIL-12 was performed using the EcoR1 and SacI-HF® restriction endonucleases (New England Biolabs, Ipswich, MA, USA). For enzymatic digestion, 1 μg of pIL-12 was mixed with 1 μL EcoR1 or SacI-HF® in 1X NEBuffer™ EcoR1 or rCutSmart™ buffer (New England Biolabs), respectively, and incubated at 37°C for 15 min in a heat block. After enzymatic digestion, the enzyme was inactivated by heating at 65°C for 20 min in a heat block. Digested DNA fragments were separated using agarose gel electrophoresis, as described above.

2.3.Microbubbles

Vevo MicroMarker™ contrast agents (Fujifilm-VisualSonics, Toronto, Canada) were prepared according to the manufacturer's instructions. These agents consist of MBs with gaseous core composed of a nitrogen and perfluorobutane mixture, encapsulated by a PEGylated phospholipid shell. The mean diameter in volume of these MBs ranges from 2.3 to 2.9 μm. The MBs were freshly reconstituted before each experiment, and the final concentration of stock solution was 2×10^9 MBs/mL. The concentration and dose of MBs used in this study were optimized in preliminary *in-vitro* and *in-vivo* experiments to ensure efficient gene delivery while maintaining cell viability and adequate ultrasound imaging performance. For *in-vitro*

experiments, MB concentrations of 2.7×10^6 MBs/mL and 5.4×10^7 MBs/mL were selected for the pDNA delivery of melanoma cell suspensions and melanoma spheroids, respectively. For *in-vivo* experiments, an amount of 2×10^6 MBs was injected intratumorally. These parameters were determined based on a balance between pDNA delivery efficiency, cell viability, US attenuation, and contrast enhancement [29, 43-45]. The optimized conditions provided a reproducible and efficient acoustic response suitable for both *in-vitro* and *in-vivo* acoustically mediated pDNA delivery assays.

2.4.Cell culture

B16F10 (ATCC-CRL-6475) murine melanoma cells were purchased from LGC Standards SARL (Molsheim, France). These cells were cultured as a monolayer in Dulbecco's modified Eagle's medium (DMEM® High W/GlutaMAX-I; ThermoFisher Scientific), supplemented with 10% fetal calf serum (FCS; Eurobio, Courtaboeuf, France) and 1% penicillin-streptomycin (10,000 U/mL; ThermoFisher Scientific).

2.5.In-vitro pIL-12 delivery in cell suspension

As previously described [44], our US device for *in-vitro* pDNA delivery in cell suspensions consisted of an arbitrary waveform generator (Agilent, Santa Clara, CA, USA) that produces a sinusoidal electrical signal composed of 40-cycle pulses repeated every 100 μs (*i.e.,* 40% duty cycle) at a central frequency of 1 MHz. Then, the signal was amplified using a power amplifier (AAP-500-0.2-6-D; ADECE, Valbonne, France) and transmitted to a 1-MHz single-element transducer (IBMF014; NDT Systems, Nashua, NH, USA) with a diameter of 12.7 mm, a natural focal distance at 27 mm, and a focal spot size of 6 mm.

For cell transfection, B16F10 cells were harvested with 0.25% trypsin-ethylenediaminetetraacetic acid (ThermoFisher Scientific) at 37°C and resuspended at a concentration of 5×10^5 cells per 1.5 mL in DMEM® High Glucose with GlutaMAX-I (ThermoFisher Scientific) supplemented with 1% FCS but without antibiotics. Cell viability

was evaluated via Trypan Blue exclusion assay and was approximately 97%. During transfection, the cell suspension was maintained at 37°C in a water bath. A volume of 1.5 mL from the cell suspension was transferred into a plastic cuvette containing a magnetic stir bar. Microbubbles (MBs; 2 μL, final concentration 2.7×10^6 MBs/mL) and pIL-12 plasmid (2.5 or 5 μL of 2 μg/μL pIL-12 solution) were added 1 min before US exposure. The cuvette was positioned at the focal point of the transducer in a degassed water tank maintained at 37°C. The suspension was gently stirred using a magnetic stir bar to ensure homogeneity during US exposure. Cells were then subjected to a peak negative pressure of 400 kPa for a total exposure time of 30 s, corresponding to the optimal acoustic parameters for *in-vitro* gene and drug delivery [44, 46].

After US exposure, 500 μL of the cell suspension was seeded in 24-well culture plates (ThermoFisher Scientific) and incubated at 37°C in a humidified atmosphere with 5% CO_2. Four hours later, the final concentration of FCS was increased to 10%, and 1% penicillin and streptomycin (10,000 U/mL) was added. The plates were then incubated as depicted above for 48 h. Transfection efficiency was assessed by measuring IL-12 secretion in the cell culture medium using a mouse IL-12 ELISA kit (ab119531, Abcam, Cambridge, UK), following the manufacturer's instructions. A 3-(4,5-dimethylthiazol-2-yl)-2,5-diphenyltetrazolium bromide (MTT) colorimetric assay (ThermoFisher Scientific) was used to assess cell viability 48 h after pIL-12 delivery, as previously reported [47].

2.6.In-vitro pIL-12 delivery in melanoma spheroids

B16F10 melanoma spheroids were generated using the hanging-drop method adapted from Akil *et al* [48]. Drops of 20 μL of cell medium supplemented with 0.5 % (v/v) methylcellulose (Biotechne, Noyal-Châtillon-sur-Seiche, France) containing 500 cells were suspended on the lid of agar-coated 24-well plates. Each well was filled with 500 μL of Dulbecco's phosphate-

buffered saline solution (ThermoFisher Scientific) to prevent evaporation. The plates were incubated at 37 °C in a humidified atmosphere with 5% CO_2 for 4 days.

Four days later, spheroids were observed under an optical microscope (EVOS^{TM} M5000 imaging system; ThermoFisher Scientific), and their area was measured using ImageJ software (NIH, Bethesda, MA, USA). As previously described [43], spheroids were washed twice with PBS and suspended in DMEM® High W/GlutaMAX-I supplemented with 1% FCS (5 spheroids per 1.5 mL). This suspension was placed in a dedicated plastic cuvette. The MBs (40 µL; final concentration of 5.4×10^7 MBs/mL) and the pIL-12 (10 or 50 µg) were mixed and added to the spheroid suspension 1 min before US exposure. The cuvette was immersed in a deionized, degassed water bath maintained 37°C, with its center positioned at the focal distance of the transducer. Subsequently, the spheroid suspension was exposed to US waves using the same device and acoustic parameters as those applied for the pIL-12 delivery in cell suspension.

Two hours later, spheroids were transferred to 96-well ULA microplates and cultured in complete cell medium supplemented with 0.5% methylcellulose. The microplates were then incubated at 37 °C in a humidified 5% CO_2 atmosphere incubator for 48 h. Spheroid growth was monitored using an optical microscope at 24 and 48 h after pIL-12 delivery. Spheroid area was quantified using ImageJ software. Finally, IL-12 secretion in the cell culture medium was assessed using ELISA.

2.7.In-vivo pDNA delivery in a mouse melanoma model

The animal study was reviewed and approved by the Animal Care and Regional Committee for Ethics in Animal Experiments, Centre Val-de-Loire, in accordance with European Directive 2010/63/EU for animal experiments. Male C57Bl6 mice (Janvier Labs, Le Genest-Saint-Isle, France) were 5 weeks old and weighed approximately 20 g before the experiments. They were housed in groups of five under temperature- and humidity-controlled conditions and a 12:12 light-dark cycle, with food and water provided *ad libitum*. Mice were acclimated to their

housing for 1 week before *in-vivo* procedures. To assess their physical conditions, mice were weighed, and their general health status (*i.e.,* respiratory deficiency, loss of locomotion, and loss of appetite) [47] as well as the coat condition [49], were monitored whenever the mice were handled.

Mice were anesthetized with 2% isoflurane in oxygen (2 L/min) administered via a facial mask. They were positioned on a thermostatically controlled pad to maintain body temperature at 37°C. While under anesthesia, the mice were shaved with an electric razor, and the skin at the injection site was cleaned. Subsequently, 100 µL of 1 × 10^6 cells in PBS was then subcutaneously injected in the left flank of each mouse using a 26G hypodermic needle (0.45 × 10 mm; Terumo Europe NV, Leuven, Belgium). As previously described [47], tumor dimensions were measured using B-mode US imaging (Vevo F2, Visualsonics-Fujifilm Inc., Toronto, Canada). Tumor volume was calculated using the following formula:

$$Tumor\ volume = \frac{length \times width \times thickness}{2}$$

A tumor volume between 50 and 75 mm^3 was used as the criterion for the pDNA delivery in tumors. Mice were randomly divided into 4 groups, with 10 mice per group. While under anesthesia, an acoustic-absorbing pad was positioned between the mice and the heating pad. Tumor nodules and the surrounding skin were carefully shaved and cleaned. Then, a mixture of 50 µL containing 50 µg pDNA (pLUC or pIL-12) and 2 × 10^6 MBs was intratumorally injected using a 30G insulin syringe (0.3 × 12.7 mm; Pikdare France, Paris, France) [29, 45]. This administration preceded US application by 5 min to allow MB diffusion within the tumor tissue. Acoustic gel, used as a coupling agent, was centrifuged to remove air bubbles (10 min, 1,500 g), and then carefully applied to the tumor. For *in-vivo* pDNA delivery, the *in-vitro* transducer was replaced with a dedicated, custom-built 1.1-MHz transducer (13 mm diameter) positioned at a natural focal distance of 27 mm, with a focal spot of 30 mm. This transducer was inserted in a dedicated degassed water-filled adaptor to ensure proper coupling with the

tumor nodule and to position the focal point at the tumor center. The tumor were then exposed to 1.1 MHz sinusoidal US waves with a pulse repetition period of 100 µs, 40 cycles per pulse, and a negative pressure of 400 kPa for 3 min, which represent the optimal acoustic parameters for *in-vivo* gene and drug delivery [44, 47].

As described above, the effects of *in-vivo* pDNA delivery on the tumor growth were assessed by measuring the tumor dimensions using B-mode US imaging [46, 47]. Luciferase expression in tumors was detected and recorded at 24 and 48 h post-gene delivery using the IVIS Lumina (Perkin Elmer, Waltham, MA, USA). Twenty minutes prior to imaging, luciferin (150 mg/kg body weight; Perkin Elmer, Waltham, MA, USA) was administered intraperitoneally. Following the injection, the mice were awoken. Five minutes post-luciferin injection, the mice were anesthetized with 2% isoflurane in oxygen (2 L/min). Bioluminescence flux was quantified as the total photons/sec in the region of interest drawn around the tumor.

2.8.Serum IL-12 ELISA assay

Blood samples were collected by cardiac puncture into serum collection tubes from the same animals used for flow cytometry analysis. The samples were allowed to coagulate for 2 h and then centrifuged at 2,000 g for 10 minutes to obtain the serum. Mouse IL-12 levels were determined using serum ELISA, following the manufacturer's instructions (ab119531, Abcam, Cambridge, UK).

2.9.Cell preparation and surface staining for flow cytometry

After dissection, tumors were processed using a standardized mechanical protocol without enzymatic digestion. Each tumor was manually dissociated on a 100 µm cell strainer (ClearLine®, DUTSCHER SAS, Bernolsheim, France) using PBS 1X supplemented with 2% FBS. Cells were centrifuged at 500 g for 5 min at room temperature. The pellet was resuspended in 1 mL of red blood cell lysis buffer for 3 min, followed by the addition of 9 mL of PBS 2% FBS to stop the reaction. After filtration through a 40 µm cell strainer (ClearLine®,

DUTSCHER SAS) and an additional centrifugation step (500 g, 5 min), cells were resuspended in PBS with 2% FBS + 2 mM EDTA (FACS buffer) for counting and surface staining.

Surface staining was performed on 1 × 10^6 cells in FACS buffer under non-permeabilizing conditions. The procedure was carried out at 4°C and in the dark to prevent internalization of membrane targets. Fc gamma receptors (FcγR) were blocked using True-Stain FcX™ (anti-mouse CD16/32; clone 93, BioLegend®, San Diego, CA, USA), followed by incubation for 20 min with antibodies from two complementary panels. Antibody clones are indicated in parentheses, and antibodies were purchased from BioLegend® apart NK1.1-BB700:

- Lymphoid panel: anti-mouse CD3-PE/Cyanine 7 (145-2C11); anti-mouse CD4-APC-A700 (GK1,5); anti-mouse CD8-Pacific Blue (53-6.7); anti-mouse CD19-BV605 (6D5); anti-mouse NK1.1-BB700 (clone PK136; BD Bioscience™, Le Pont de Claix, France); anti-mouse CD69-FITC (H1.2F3); and anti-mouse CD45- APC/Cyanine 7 (30-f11).
- Myeloid panel: anti-mouse CD11b-APC-A700 (M1/70) anti-mouse CD11c-BV605 (NA18); anti-mouse Ly6C-PE-Cy7 (hk1.4); anti-mouse Ly6G-BV421 (1A8) anti-mouse MHC-II-PerCP/Cy5.5 (M5/114,15,2); anti-mouse CD86-FITC (GL1); and anti-mouse CD45-APC/Cyanine 7 (30-f11).

Data were acquired using a flow cytometer CytoFLEX S™ (4 lasers B-R-V-N, Beckman Coulter Inc., München, Germany) and analyzed using Kaluza Analysis™ software version 2.2.1 (Beckman Coulter).

2.10. Statistical analysis

Statistical analyses were performed using GraphPad Prism 10 software (GraphPad Software Inc., La Jolla, CA, USA). All quantitative data were presented as mean ± SD, unless otherwise indicated. Statistical tests were described in the relevant captions. Values of $P < 0.05$ were considered significant and were adjusted for multiple comparisons, as indicated in the legends.

3. Results

3.1.In-vitro pIL-12 delivery in B16F10 cell suspension

pIL-12 (also known as pCpGfree-mIL12), which encodes the murine interleukine-12 (**Figure 1A**), was produced and purified from transformed *E. coli* GT115 cells using the EndoFree Plasmid purification system. Notably, endotoxins reduced the *in-vitro* and *in-vivo* transfection efficiencies [50] and induced non-specific immune activation *in-vivo* [51]. The purification yield was 7.5 mg. pIL-12 was predominantly present in the supercoiled form (90 ± 1%), with smaller proportions in the open-circular (9 ± 1%) and linear (1 ± 1%) forms (**Figure 1B**). No bacterial genomic DNA contamination was detected in the pIL-12 solution. To confirm its identity, pIL-12 was digested with the restriction enzymes EcoR1 and Sac1 (**Figure 1B**). As expected, the EcoR1 digestion generated two DNA fragments (1.9 and 2.7 kb), along with a third fragment corresponding to the linearized pIL-12 (~4.5 kb). Sac1 digestion of pIL-12 produced two DNA fragments (1.4 and 3.2 kb). Altogether, these results confirm that pIL-12 was produced at a high yield and displayed high purity without contamination.

In-vitro pIL-12 delivery using MB-assisted US was assessed by measuring of IL-12 concentrated secreted in the cell culture medium (*i.e.,* transfection efficiency) 48 h post-treatment using an ELISA. Simple incubation of pIL-12 (5 or 10 μg) with the B16F10 cells did not result in the production and the secretion of IL-12 into the cell medium (**Figure 1C**). In contrast, acoustically mediated delivery of 5 μg pIL-12 in cell suspension induced substantial IL-12 production (1429 ± 125 pg/mL). Doubling the pIL-12 concentration further increased IL-12 levels (2352 ± 125 pg/mL; $P < 0.05$ vs. 5 μg pIL-12). The effect of pIL-12 delivery on cell viability using MB-assisted US was assessed via MTT assay at 48 h post-treatment (**Figure 1D**). Exposure of cell suspensions to MB-assisted US alone or to pIL-12 (5 or 10 μg) alone did not significantly affect cell viability ($P > 0.05$). However, acoustically mediated delivery of 5 or 10 μg of pIL-12 led to a slight but significant decrease in cell viability (78 ± 2% and 85 ± 3%, respectively) compared to the control groups ($P < 0.05$). These findings reveal that pIL-12

was functional and that MB-assisted US enables efficient and safe delivery of pIL-12 in B16F10 cell suspension.

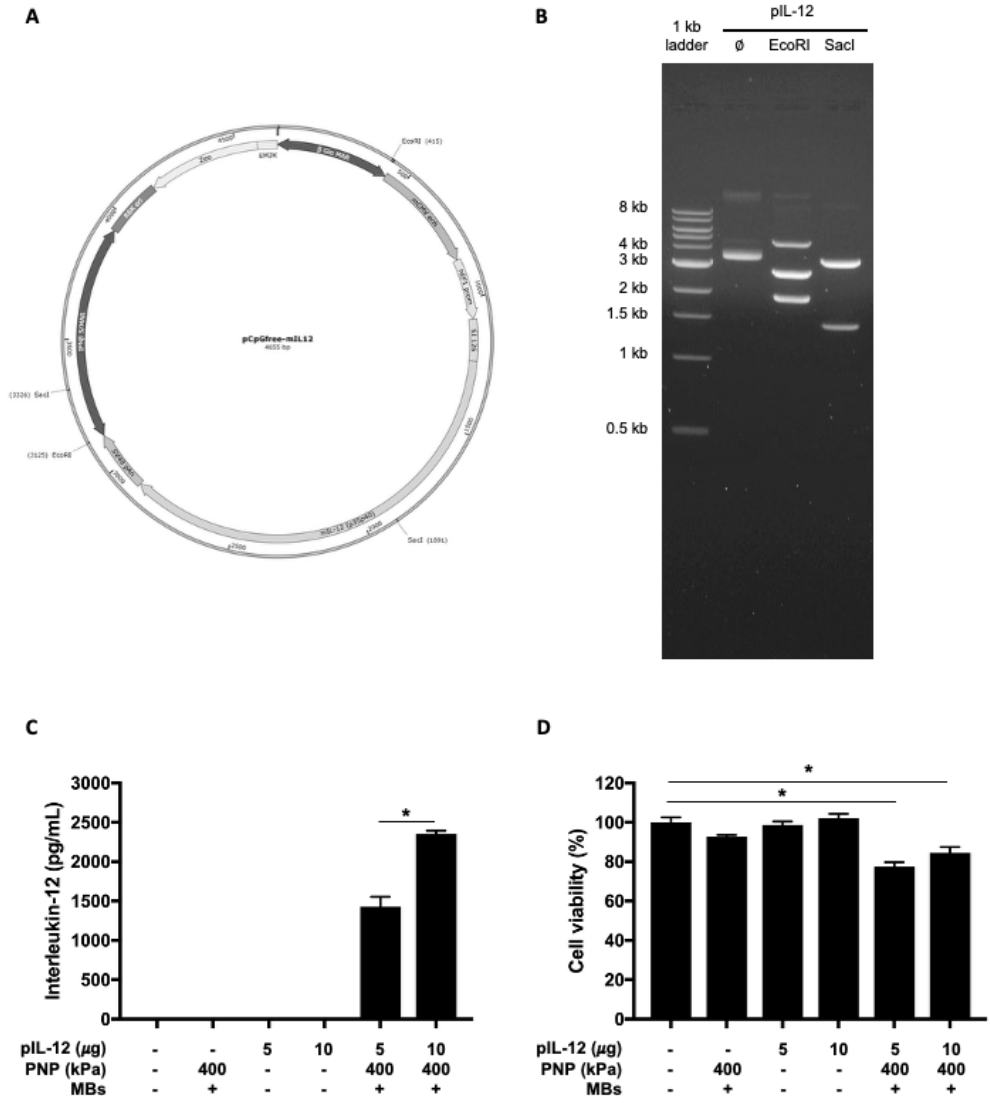

Figure 1. *In-vitro* pIL-12 delivery in B16F10 cell suspension using MB-assisted US. (A) pCpGfree-mIL12 map (created with SnapGene®); (B) Restriction enzyme digestion analysis of pIL-12 by agarose gel electrophoresis. Lane 1 kb ladder: DNA molecular weight marker; lane Ø: undigested pIL-12; lane EcoR1: pIL12 digested with EcoR1 restriction enzyme; lane Sac1: pIL12 digested with Sac1 restriction enzyme; (C) Transfection efficiency of B16F10 cells; cell suspensions incubated with pIL-12 (5 or 10 μg) and MBs and exposed to US. Secretion of IL-12 in the cell culture medium was assessed 48 h post-treatment using ELISA; (D) Cell viability

of transfected B16F10 cells was assessed using an MTT assay 48 h post-*in-vitro* pIL-12 delivery. All data are expressed as mean ± SD calculated from five independent experiments. Statistical analysis was performed using the One-way ANOVA with Tukey's multiple comparison test. Adjusted P value was $*P < 0.05$.

3.2.In-vitro pIL-12 delivery in melanoma spheroids

pIL-12 was acoustically delivered to B16F10 melanoma spheroids at two doses: 10 μg (the higher concentration used *in-vitro* in cell suspension) or 50 μg (the concentration used *in-vivo*), thereby partially mimicking the *in-vivo* context. The concentration of IL-12 secreted in the cell medium (*i.e.,* transfection efficiency) was measured 48 h post-treatment using ELISA (**Figure 2A**). Melanoma spheroid growth was assessed using optical microscopy before (day 4) and after (days 5 and 6) *in-vitro* pIL-12 delivery (**Figures 2B & 2C**).

Treatment of melanoma spheroids with 10 and 50 μg of pIL-12 alone induced no or minimal (0 and 7.5 ± 5 pg/mL) production and secretion of IL-12 into the cell culture medium, respectively (**Figure 2A**). In contrast, acoustically mediated delivery of 10 and 50 μg of pIL-12 in melanoma spheroids resulted in significant IL-12 production in cell culture medium (*i.e.,* 131 ± 7 and 250 ± 60 pg/mL; $P < 0.05$) compared to their respective control groups ($P < 0.001$). Regardless of the pIL-12 concentrations, exposure of melanoma spheroids to either pIL-12 alone, MB-assisted US alone, or pIL-12 in combination with MB-assisted US did not significantly affect the spheroid growth ($P > 0.05$). These results demonstrate that MB-assisted US is an efficient modality for delivering pIL-12 into melanoma spheroids without inducing cell damage.

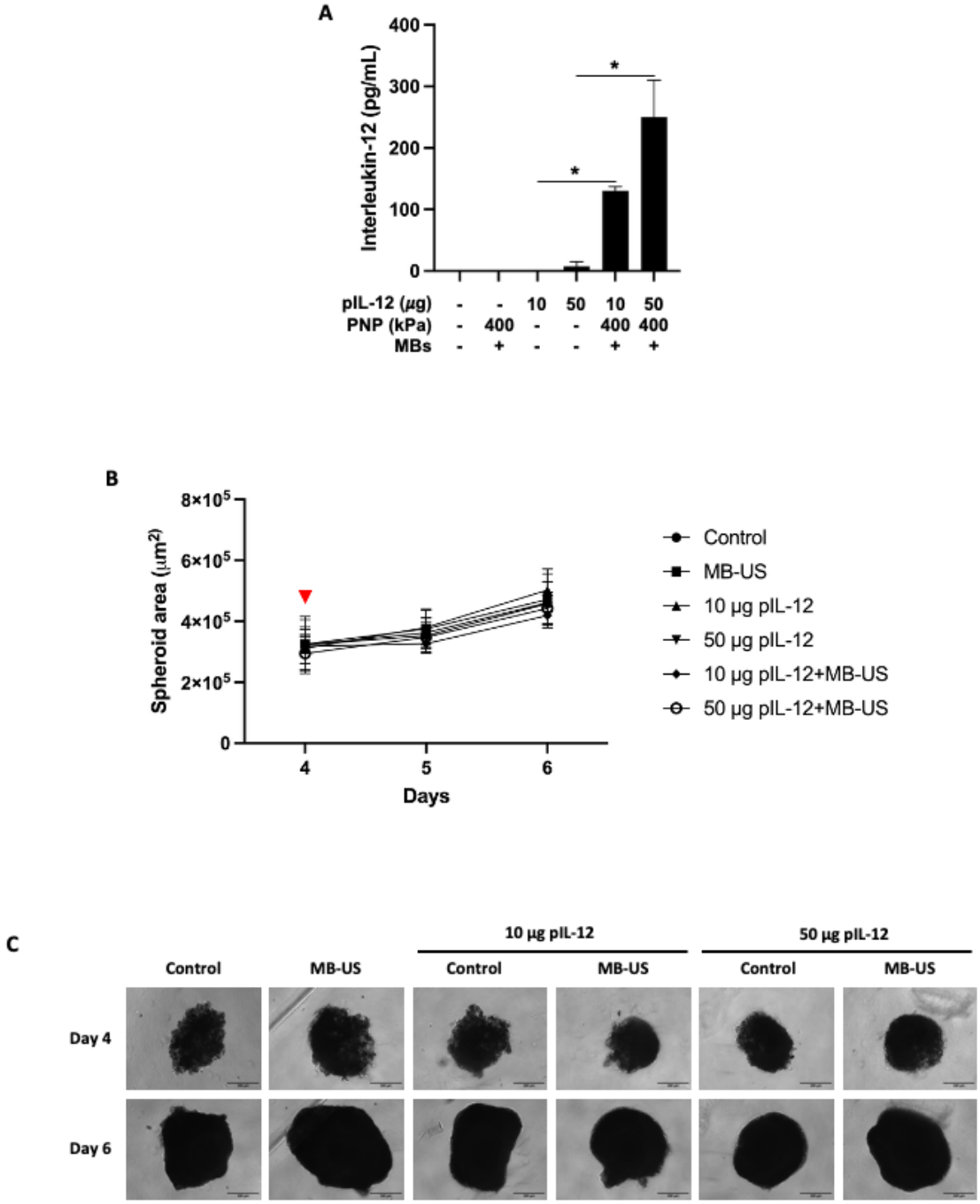

Figure 2. *In-vitro* pIL-12 delivery in B16F10 melanoma spheroids using MB-assisted US. (A) Transfection efficiency of melanoma spheroids: spheroid suspension was incubated with pIL-12 (10 or 50 μg) and MBs, and then exposed to US. Secretion of IL-12 in the cell culture medium was assessed 48 h post-treatment using ELISA; (B) Growth of transfected melanoma spheroids: spheroid growth was assessed using an optical microscope before (day 4) and after (days 5 and 6) *in-vitro* pIL-12 delivery. All data were expressed as mean ± SD and calculated

from five independent experiments. Statistical analysis was performed using the One-way ANOVA with Tukey's multiple comparison test. Adjusted P value was *$P < 0.05$; (C) Representative images of transfected melanoma spheroids. Scale bar indicates 300 μm.

3.3.In-vivo assessment of acoustically mediated pDNA delivery: Validation with pLUC and therapeutic evaluation with pIL-12 in a melanoma mouse model

To evaluate the feasibility of *in-vivo* pDNA delivery by MB-assisted US, the delivery and expression of a luciferase reported plasmid (pLUC) were assessed in a B16F10 melanoma mouse model prior to investigating the therapeutic efficacy of pIL-12 delivery. Melanoma tumors were thus treated once their volume reached 50 mm^3 (**Figures 3A &3B**). A solution of pLUC (50 μg) and MBs (2×10^6 MBs) was co-injected intratumorally 5 min prior to US application to allow diffusion of MBs and pLUC within the tumor tissue (pLUC+MB-US; **Figure 3C**). Additionally, a group of melanoma tumors received an i.t. injection of pLUC alone and served as the control group (pLUC). Luciferase expression in the melanoma tumors was assessed using bioluminescence imaging at 24 and 48 h post-pLUC delivery (**Figure 3D**). The effects of *in-vivo* acoustically mediated pLUC delivery on mouse quality of life were assessed by a qualitative analysis of general health status and a quantitative analysis of body weight (**Figure 3E**) and coat condition (**Figure 3F**).

Intratumoral administration of pLUC alone did not induce luciferase expression in the tumor tissue (**Figure 3D**). In contrast, acoustically mediated pLUC delivery led to a significant increase in luciferase expression in the tumor tissue 24 h post-treatment (*i.e.,* $6 \pm 2 \times 10^5$ photons/sec), compared to pLUC alone (****$P < 0.0001$). At 48 h, luciferase expression slightly declined ($P > 0.05$; compared to 24 h). Moreover, no variation in overall general health or physical condition was observed between mice receiving pLUC treatment alone and those receiving acoustically mediated pLUC delivery. Both mouse groups similarly exhibited a slight gain in body weight (1-2 g on average, ~10% of initial body weight after 12 days; **Figure 3E**)

and a minimal comparable increase in coat condition score (0.5 ± 0.1 and 0.4 ± 0.1; $P > 0.05$) (**Figure 3F**). Altogether, these results reveal that MB-assisted US enhances i.t. delivery of pLUC without inducing adverse side effects.

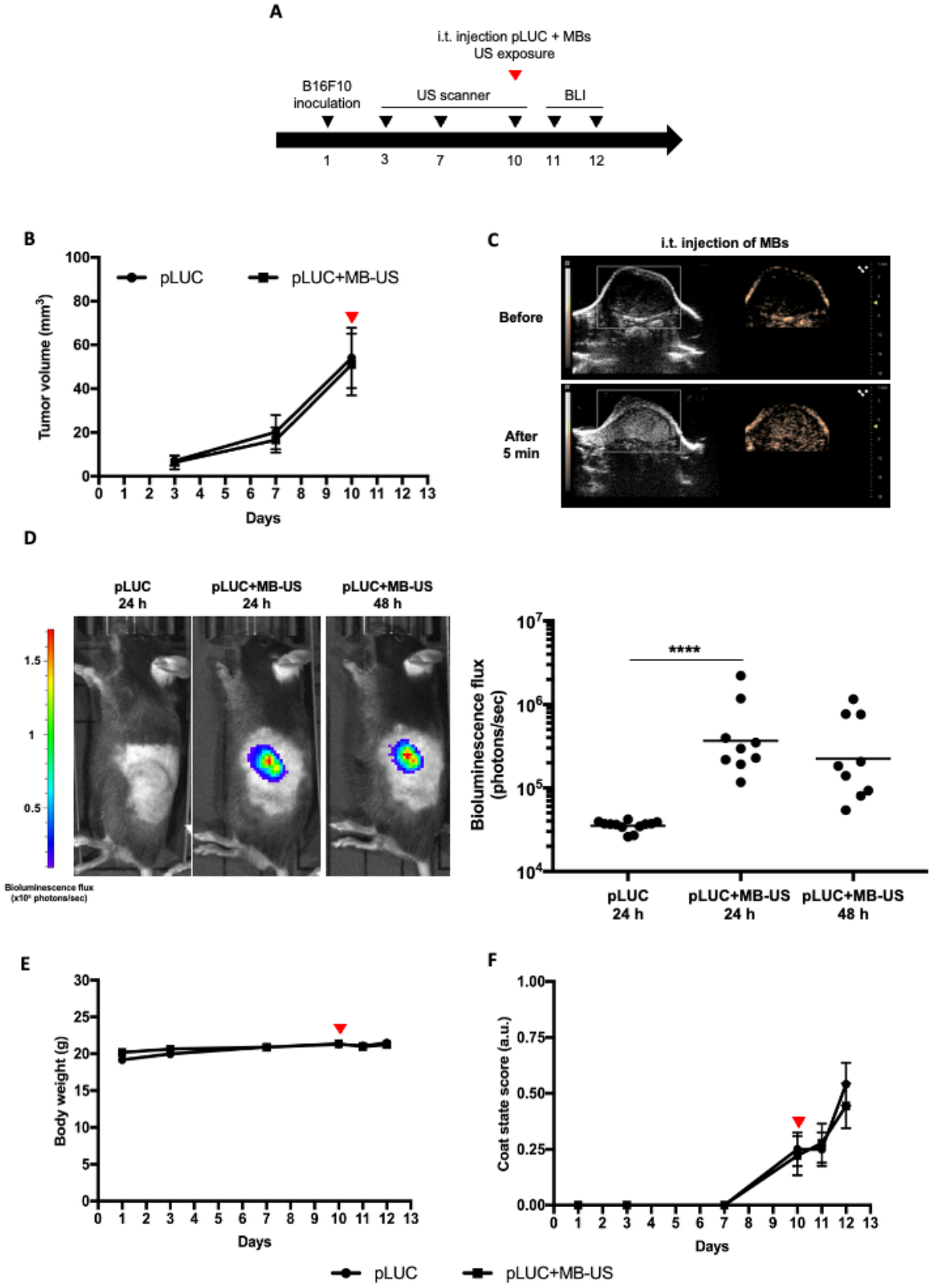

Figure 3. *In-vivo* pLUC delivery in a mouse B16F10 melanoma model using MB-assisted US. (A) Timeline of the experiments for acoustically mediated pLUC delivery in mouse

melanoma model. Tumors were treated (red arrow) either by i.t. injection of pLUC alone (pLUC) or by i.t. coadministration of pLUC and MBs, followed by US exposure (pLUC+MB-US); (B) Growth of *in-vivo* B16F10 melanoma tumors: volume was monitored using anatomical US imaging; (C) US imaging of i.t. MBs bioavailability: B-mode (left image) and contrast-enhanced US (CEUS) imaging (right image) of i.t. MB distribution before and after their i.t. administration (50 µL containing 2×10^6 MBs); (D) Quantitative bioluminescence imaging of luciferase expression inside the melanoma tumor: A mixture of 50 µL containing 50 µg pLUC and 2×10^6 MBs were intratumorally coadministered. This injection preceded the US application by 5 min to allow for MB diffusion inside the tumor tissue. Luciferase expression in the melanoma tumors was detected and recorded 24 and 48 h post-treatment; (E) Effect(s) of acoustically mediated pLUC delivery on mouse body weight; (F) Effect(s) of acoustically mediated pLUC delivery on mouse coat state. This score was measured whenever the mice were handled. All data were expressed as mean ± SD and calculated from ten mice. Statistical analysis was performed using the Two-way ANOVA with Tukey's multiple-comparisons test. Adjusted P value was $*P < 0.05$.

Following the *in-vivo* validation of efficient pDNA using the pLUC, the therapeutic efficacy of acoustically mediated pIL-12 delivery was subsequently evaluated in the same melanoma model. As shown in **Figure 4A**, melanoma tumors were either left untreated (Ctrl), exposed to US following i.t. injection of MBs (MB-US), received i.t. administration of pIL-12 (pIL-12) alone, or treated with i.t. coadministration of pIL-12 and MBs followed by US exposure (pIL-12+MB-US; **Figure 4A**). The therapeutic efficacy of *in-vivo* pIL-12 delivery with or without MB-assisted US was monitored using anatomical US imaging (**Figure 4B**). As described above, the effects of *in-vivo* acoustically mediated pIL-12 delivery on the mouse weight and coat condition were also assessed (**Figure 4C & 4D**).

Intratumoral administration of pIL-12 alone did not affect the tumor growth compared to the control group (pIL-12 *vs* Ctrl; $P > 0.05$) (**Figure 4B**). Similarly, exposure of tumors to MB-assisted US alone did not disrupt tumor growth compared to the control group and pIL-12 treatment (MB-US *vs* Ctrl or *vs* pIL-12; $P > 0.05$) (**Figure 4B**). In contrast, acoustically mediated pIL-12 delivery resulted in a significant decrease in tumor volume compared to control group (pIL-12+MB-US *vs* Ctrl; $^{***}P < 0.001$) and other experimental groups (pIL-12+MB-US *vs* pIL-12 or *vs* MB-US; $^{***}P < 0.001$) (**Figure 4B**). By day 15, the average tumor volume in the pIL-12+MB-US group was 2.5-fold lower than that of the control (*i.e.,* Ctrl) and other experimental groups (*i.e.,* pIL-12 and MB-US). These results indicate that *in-vivo* acoustically mediated pIL-12 delivery effectively inhibits tumor growth.

Moreover, mice that were untreated (Ctrl), exposed to US after i.t. injection of MBs (MB-US), or administered pIL-12 alone did not show an overall deterioration of their general health conditions (*e.g.,* respiratory deficiency and loss of appetite). They exhibited a body weight gain of approximately 3 g (*i.e.,* 13% of initial body weight on day 15) (**Figure 4C**). However, they displayed physical impairments such as locomotion and coat condition (*i.e.,* a coat state score greater than 1; **Figure 4D**), which are likely due to the tumor growth. In contrast, mice treated with pIL-12+MB-US exhibited neither an overall deterioration of their health status nor loss of body weight (**Figure 4C**). Notably, these mice exhibited normal locomotion and a significantly lower coat condition score (0.4 ± 0.1) than those of control (2.0 ± 0.3 for Ctrl) and experimental mice groups (1.6 ± 0.3 for pIL-12 and 1.4 ± 0.3 for MB-US) at the 15^{th} day ($^{***}P < 0.001$). Altogether, these data suggest that the slowed tumor growth induced by acoustically mediated pIL-12 delivery was associated with improved overall health in mice.

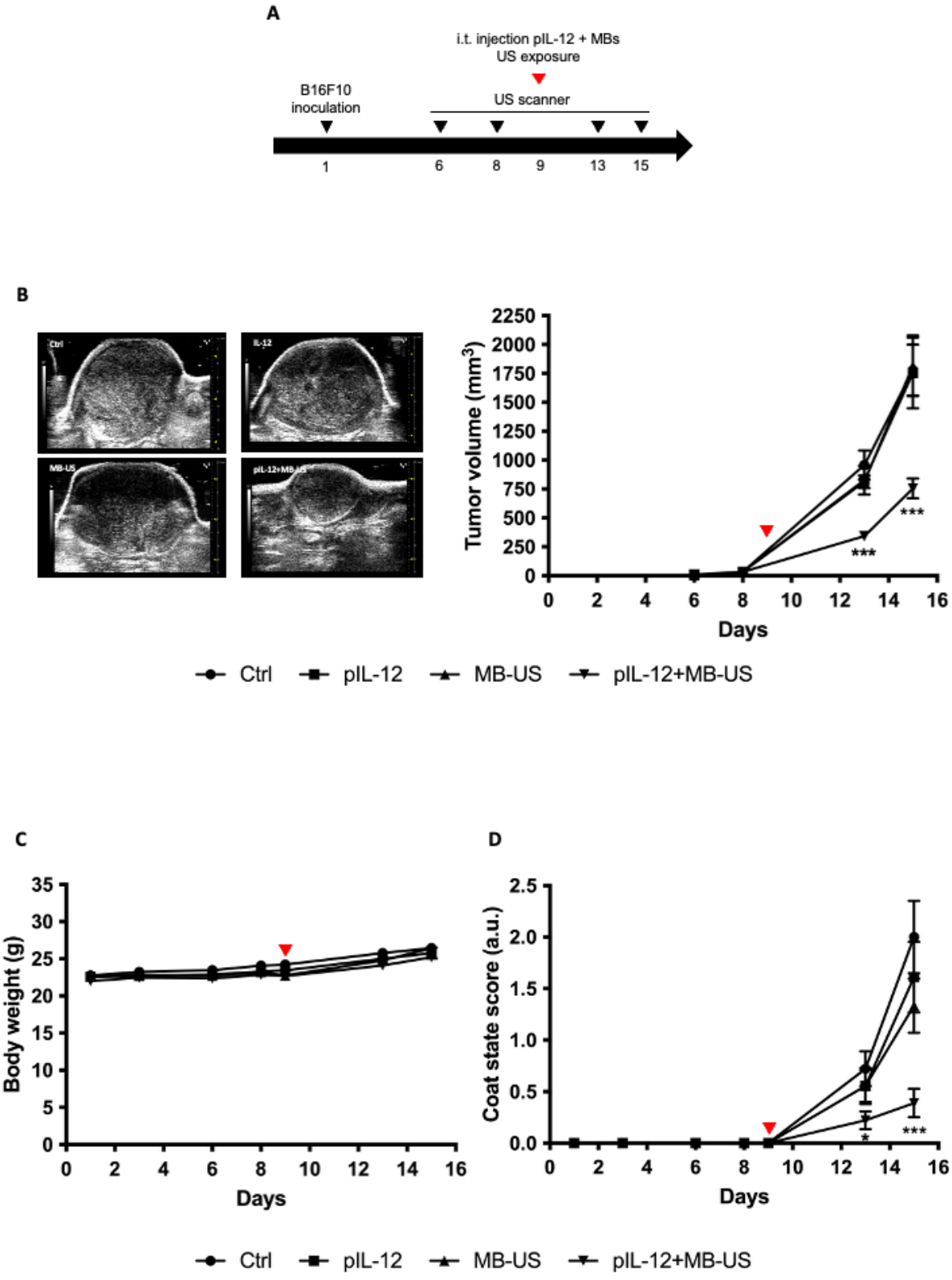

Figure 4. *In-vivo* pIL-12 delivery in a mouse B16F10 melanoma model using MB-assisted US. (A) Timeline of the experiments for acoustically mediated pIL-12 delivery in a mouse melanoma model. Tumors were treated (red arrow) either by i.t. administration of pIL-12 alone

(pIL-12), i.t. injection of MBs followed by US exposure (MB-US), or by an i.t. coadministration of pIL-12 and MBs followed by US exposure (pIL-12+MB-US). A group of tumors left untreated served as the control group (Ctrl); (B) Growth of B16F10 melanoma tumors *in-vivo*, monitored using anatomical US imaging; (C) Effect(s) of acoustically mediated pIL-12 delivery on mouse body weight. Mice were weighed whenever they were handled; (D) Effect(s) of acoustically mediated pIL-12 delivery on mouse coat condition. Coat score was measured whenever mice were handled. All data are expressed as mean ± SD and were calculated from ten mice. Statistical analysis was performed using the Two-way ANOVA with Tukey's multiple-comparisons test. Adjusted P value was $*P < 0.05$.

3.4.Immunomodulatory response of acoustically mediated pIL-12 delivery

The expected outcome of pIL-12 delivery using MB-assisted US is an increase in serum mIL-12 levels. Therefore, to evaluate whether i.t. acoustically mediated delivery of pIL-12 also induces systemic mIL-12 release, serum mIL-12 concentrations were measured using ELISA 48 h post-pIL-12 administration. The results revealed that the i.t. acoustically mediated delivery of pIL-12 significantly increased serum mIL-12 concentrations by 5-fold and 13-fold compared to the i.t. pIL-12 injection alone ($P < 0.05$) or the control group ($P < 0.01$), respectively (**Figure 5B**). These results indicate that *in-vivo* acoustically mediated pIL-12 delivery enhances the production and systemic secretion of IL-12.

To evaluate the immunomodulatory effects of acoustically mediated pIL-12 delivery, flow cytometry was performed on five tumors per group (Ctrl, pIL-12, and pIL-12+MB-US). The analysis included quantification of major i.t. immune populations, T lymphocytes and subsets, B lymphocytes, NK cells, monocytes, neutrophils, and dendritic cells, as well as two activation markers: CD69 for T and NK cells, and CD86 for myeloid cells. Among all assessed parameters, only NK cell frequency and activation were significantly influenced by the treatment. A significant increase in NK cell frequency was observed in the pIL-12+MB-US

group compared to the control group ($P < 0.05$), while no differences were detected between the pIL-12 group and the other groups ($P > 0.05$; **Figure 5C**). Similarly, CD69 expression on NK cells was significantly higher in the pIL-12+MB-US group compared to both the control and pIL-12 groups ($P < 0.05$), with no difference observed between the latter two ($P > 0.05$; **Figure 5D).**

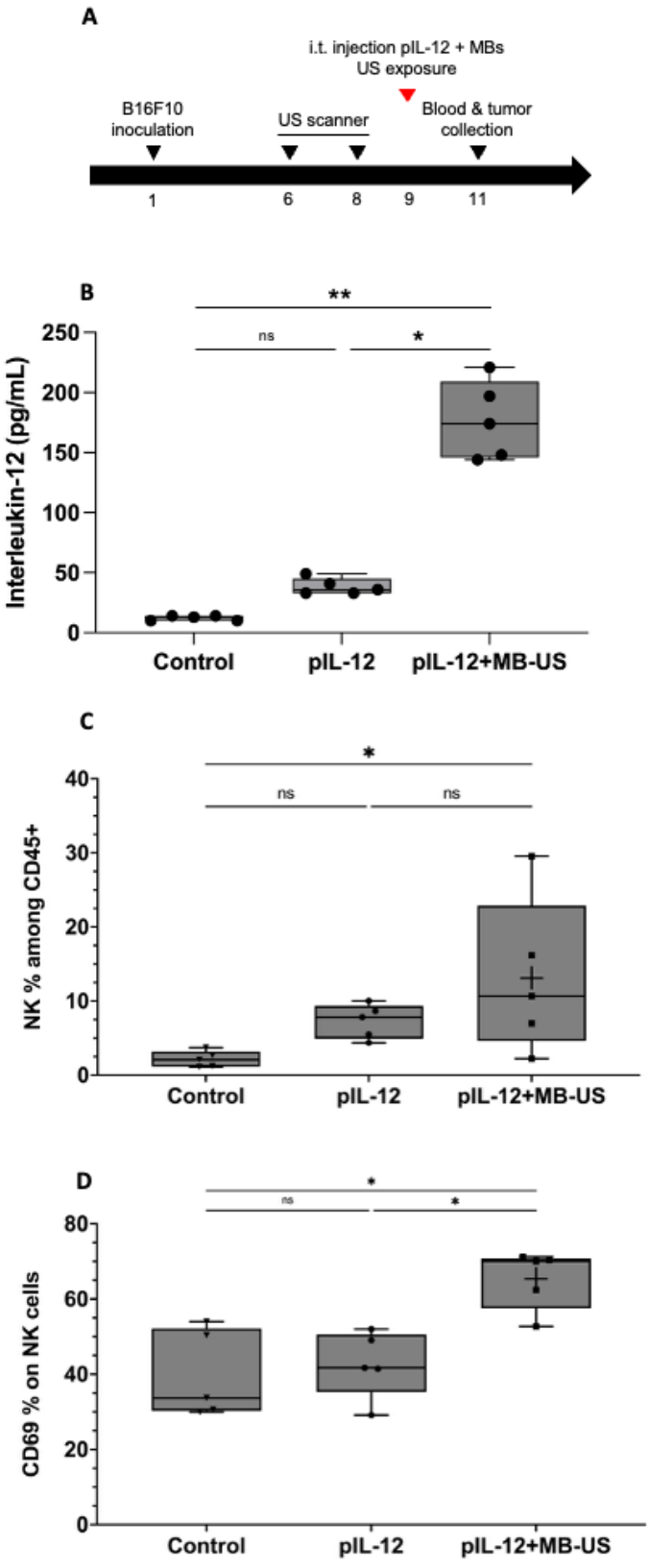

Figure 5. Immunomodulatory effects of acoustically mediated pIL-12 delivery. (A) Experimental timeline for acoustically mediated pIL-12 delivery in a mouse melanoma model.

Tumors were treated (red arrow) either by i.t. administration of pIL-12 alone (pIL-12), by i.t. injection of MBs followed by US exposure (MB-US), or by an i.t. coadministration of pIL-12 and MBs followed by US exposure (pIL-12+MB-US). A group of tumors left untreated served as the control group (Ctrl); (B) Serum concentration of mIL-12. Secretion of IL-12 in the blood was assessed 48 h post-pIL-12 delivery using ELISA; (C) Frequency of NK cells expressed as a percentage of $CD45^+$ cells in tumors; (D) CD69 expression on the surface of intratumoral NK cells in tumors. Data are presented as median with minimum and maximum values. Statistical significance was determined using the Kruskal–Wallis test followed by Dunn's post hoc test for multiple comparisons. $P < 0.05$ was considered statistically significant. "ns" indicates non-significant differences; * indicates $P < 0.05$ and ** indicates $P < 0.01$.

4. Discussion

The present study aimed to assess the efficacy of MB-assisted US for pIL-12 delivery in both *in-vitro* (*i.e.,* suspension of melanoma cells and melanoma spheroids) and *in-vivo* melanoma models. *In-vitro,* acoustically mediated pIL-12 delivery resulted in significant production and secretion of IL-12 in the cell culture medium (**Figures 1C & 2A**) without inducing irreversible cell damage (**Figures 1D & 2B, C**), compared with pIL-12 treatment alone (**Figures 1 & 2**). These findings indirectly suggest that the increase in IL-12 production could be ascribed to enhanced intracellular uptake of pIL-12 via acoustically induced hydrophilic membrane pores and its subsequent expression by the melanoma cells. Indeed, previous investigations reported that MB-assisted US reversibly increases the native membrane permeability of tumor cells through the formation of transient hydrophilic membrane nanopores [52-54]. The intercellular uptake of exogenous molecules, including nucleic acids (*i.e.,* pDNA, siRNA, and miRNA), chemotherapeutic drugs, antibiotics, and antibodies, relies on passive diffusion through these membrane pores, allowing these molecules to freely access the cytoplasm of tumor cells [55, 56]. Moreover, MB-assisted US was more efficient at delivering pIL-12 in melanoma cell

suspensions than in melanoma spheroids under similar experimental conditions (**Figures 1 & 2**). Indeed, exposure of cell suspension to MB-assisted US in the presence of 10 μg pIL-12 resulted in an 18-fold increase in IL-12 levels compared to acoustically mediated pIL-12 delivery in melanoma spheroids. As previously described [57], the difference in IL-12 levels could be attributed to more efficient membrane permeabilization and pIL-12 delivery in cell suspension compared to spheroids. Indeed, pIL-12 and MBs have greater access to all melanoma cells in a suspension of individual cells than in the spheroids. These spheroids are *in-vitro* three-dimensional tumor models that partly reflect tumor architecture and heterogeneity [58, 59]. The high density and/or the dense extracellular matrix of melanoma cells might restrict the diffusion of pIL-12 and MBs into spheroids, inducing the permeabilization and the transfection of only a small number of cells primarily located in the peripheral layers of the spheroids [57]. *In-vitro* studies using low molecular weight and fluorescent markers (*e.g.,* propidium iodide, dextrans, doxorubicin and nanoparticles) have confirmed that MB-assisted US permeabilizes and delivers such molecules to peripheral tumor cells in spheroids [43, 60, 61]. Since these molecules are not pDNA, reporter gene-encoding pDNA or fluorescently labeled pDNA could be used to more thoroughly investigate this hypothesis [62, 63].

Subsequently, our *in-vivo* results demonstrated that MB-assisted US delivery of pIL-12 significantly reduced tumor growth compared to pIL-12 treatment alone (**Figures 3 & 4**). In agreement with previous studies [29, 45], we hypothesize that i.t. injection of a mixture of pIL-12 and MBs may ensure their diffusion throughout the tumor, reaching melanoma cells, fibroblasts, immune cells, and other cell types. Subsequent exposure of the melanoma tumor to US may then activate the MBs, permeabilizing the cells and enhancing the intracellular delivery of pIL-12 [24, 64, 65]. In future investigations, the i.t. distribution and identification of transfected cell populations will be examined by histology and flow cytometry following immunolabeling with cell type-specific antibodies after acoustically mediated delivery of

pDNA encoding enhanced green fluorescent protein (eGFP). Consistent with previous reports [66, 67], the efficacy of i.t. pDNA delivery could be correlated with MB cavitation activity measured in real time during US exposure using a passive cavitation detection system. Such investigations would help clarify how acoustic activity relates to transfection efficiency and subsequent IL-12 expression. In the present work, transfected cells produced and secreted IL-12 (**Figure 5B**), thereby activating the anti-tumoral immune response through NK cell recruitment and activation in the tumor microenvironment (**Figure 5C & 5D**) [12, 14, 15, 42]. In addition to enhancing pDNA uptake, MB cavitation generated under our US conditions may also induce mechanical effects on tumor cells and stromal structures. Cavitation activity can produce transient membrane disruption, shear stress and localized microvascular perturbation, leading to the release of tumor antigens, nucleic acids and other damage-associated molecular patterns (DAMPs). Such danger signals are known to activate type I interferon pathways in various cell types, including NK cells, macrophages, fibroblasts, endothelial cells and lymphocytes, thereby promoting the recruitment and activation of cytotoxic immune populations [68]. Consistent with these mechanisms, US-mediated cytokine or pDNA delivery has been shown to enhance T-cell infiltration at both local and distant tumor sites [29] and to potentiate antitumor immunity when used as an acoustic DNA vaccination strategy [45]. Although cavitation-induced tissue perturbation was not quantified in the present study, these biophysical effects are compatible with the enhanced NK-cell recruitment observed in our model. Future work will characterize the extent of cavitation-induced tissue remodeling and DAMP signaling under our US conditions to better define their contribution to the immunological cascade initiated by IL-12 expression. Together, these observations illustrate the capacity of acoustically mediated pIL-12 delivery to trigger local cytokine production. Beyond this direct activation, IL-12 induces a broader set of coordinated immunological pathways within the tumor microenvironment that further contribute to tumor control. Upon

binding to its heterodimeric receptor (IL-12Rβ1/β2) on T cells, NK cells, and macrophages, IL-12 activates the JAK2/TYK2–STAT4 signaling pathway, resulting in robust IFN-γ secretion. IFN-γ amplifies local inflammation and drives the production of CXCL9 and CXCL10, chemokines that promote the recruitment, retention, and activation of cytotoxic T lymphocytes and NK cells, thereby establishing a self-sustaining IL-12–IFN-γ–CXCL9/10 feedback loop [9]. In parallel, IL-12 and IFN-γ promote macrophage polarization towards a pro-inflammatory M1 phenotype characterized by elevated iNOS and TNF-α expression while limiting M2-type features [14, 15, 69]. These cytokines also enhance antigen visibility by increasing MHC class I and II expression on tumor and antigen-presenting cells, improving T-cell activation and priming [9, 15, 70]. Collectively, these mechanisms reinforce antitumor effector functions and contribute to durable tumor suppression [13]. Therapeutic cancer vaccines also aim to stimulate strong Th1-oriented immunity, often through systemic delivery of tumor antigens formulated with adjuvants that promote IL-12 and IFN-γ production. Although these strategies can effectively prime cytotoxic T-cell responses, they generally require repeated immunizations, rely on efficient antigen presentation in secondary lymphoid organs, and may induce off-target inflammation. In contrast, MB-assisted US provides a non-invasive and spatially restricted method to deliver pIL-12 directly within the tumor microenvironment, ensuring high local cytokine expression while limiting systemic exposure and toxicity. By bypassing the need for antigen formulation and systemic immune priming, this approach offers a practical advantage over vaccine-based strategies, achieving rapid and concentrated immunostimulation at the tumor site. Similarly, recent preclinical studies reported that MB-assisted US effectively delivered pDNA encoding IFN-γ and granulocyte-macrophage colony-stimulating factor into orthotopic breast tumors in mice, resulting in a significant reduction in tumor growth by stimulating anti-tumoral immune responses [29, 45]. In addition to its therapeutic relevance, the protocol established in this study provides a versatile framework for i.t. transfection of other

cytokine-encoding pDNAs. MB-assisted US offers precise spatial targeting, non-invasive, high local gene expression, and minimal systemic exposure, making it well suited for dissecting the isolated contributions of individual interleukins as well as potential synergistic interactions between complementary cytokines. This modularity positions our approach as a practical platform for future investigations aiming to explore combinations of immunostimulatory pathways within the tumor microenvironment. Altogether these results confirm that MB-assisted US is a promising modality for the *in-vivo* delivery of pDNA encoding immunostimulatory molecules.

Nevertheless, while i.t. administration of both agents using US guidance is feasible in clinical settings for the treatment of superficial tumors, such as skin and breast tumors, it cannot be considered the most conventional route in routine clinical practice [1]. The i.t. route circumvents the blood-tumor barrier and the tumoral interstitial pressure and allows the direct injection of large amounts of pDNA [71]. However, this route has two main limitations: the injected volume and its restriction to superficial tumors [72]. For the treatment of superficial and deep-seated tumors, i.v. injection is currently the simplest and safest method used in clinical practice for administering MBs and therapeutic molecules, including pDNA [71, 72]. However, the main limitation of this administration route is the rapid enzymatic degradation of pDNA, which necessitates i.v. injection of a high dose of pDNA. To overcome this issue, pDNA is typically complexed with cationic lipids or polymers [73]. These complexes are then co-injected with MBs, and their respective doses are handled independently prior to their i.v. administration. Another option is to load pDNA on MBs during their assembly or to incubate pDNA with cationic MBs [20, 30]. However, in this case, the respective concentrations of MBs and pDNA are interdependent. Therefore, further studies are required to compare these administration routes for acoustically mediated delivery of pDNA encoding immunostimulatory molecules in murine models of primary and metastatic melanoma.

Furthermore, our preclinical results showed that although tumor growth in the control groups was not associated with a significant deterioration of overall physical condition (*e.g.,* respiratory failure, loss of appetite, and loss of body weight), locomotion impairments and deteriorations of coat condition were observed (**Figure 4**). However, the acoustically mediated delivery of pIL-12 into the tumor significantly reduced these locomotor impairments and coat deterioration, suggesting that this therapeutic strategy improved the overall health of the mice (**Figure 4**). In addition, these *in-vivo* results revealed that acoustically mediated delivery of pIL-12 did not induce adverse side effects, demonstrating that this protocol was well tolerated and safe, which is in agreement with previous studies [29, 45-47].

Our *in-vivo* results demonstrated that acoustically mediated delivery of pIL-12 significantly increased systemic and i.t. IL-12 levels, promoted NK cell recruitment and activation within the tumor microenvironment, and resulted in a marked reduction in tumor volume. These findings confirm that this strategy elicits a potent antitumor immune response while maintaining good overall tolerance. To place these results in context, the therapeutic efficacy of our approach can be compared with previously reported IL-12 delivery strategies based on electroporation. Electroporation (EP) has been extensively used for intratumoral delivery of IL-12 in melanoma models and has consistently shown potent therapeutic efficacy. In B16-F10 melanoma, i.t pIL-12 electrotransfer induced complete tumor regression in 47–80% of treated mice and conferred long-term protection against tumor rechallenge [74, 75]. These effects were associated with strong local expression of IL-12 and IFN-γ, $CD8^+$ T-cell and NK-cell recruitment, and perforin/granzyme-mediated cytotoxicity [76]. Combination strategies, such as electro-chemo-gene therapy with bleomycin or co-delivery of suicide genes, further enhanced antitumor responses and prevented metastasis [76, 77]. Clinical translation of this approach confirmed its capacity to activate tumor-specific immunity and to improve responses to immune checkpoint inhibitors in advanced melanoma [78]. Nevertheless, EP requires direct

electrode contact and generates transient but painful muscle contractions and tissue damage, which limit its repeatability and clinical versatility. In contrast, MB-assisted US allows non-invasive, spatially targeted, and repeatable delivery of therapeutic pDNA [79]. Beyond pDNA, MB-assisted US has successfully enhanced the delivery of chemotherapeutic agents (*e.g.,* doxorubicin, paclitaxel) [80], oncolytic virus [81], and immunostimulatory cytokines such as IL-2, TNF-α, and IFN-β [82], leading to tumor growth inhibition and immune activation in several preclinical cancer models. The present study demonstrates that acoustically mediated delivery of pIL-12 achieves a magnitude of tumor growth inhibition comparable to that reported with electroporation, while avoiding tissue injury and preserving animal well-being. These findings highlight MB-assisted US as a clinically attractive and safe alternative for localized immunogene therapy of melanoma.

Our *in-vivo* therapeutic scheme could likely be optimized by adjusting US settings (*e.g.,* acoustic pressure and exposure period) and pIL-12 (*e.g.,* concentration and administration route) and MB-related parameters (*e.g.,* soft *versus* hard-shelled MB, free MBs *versus* pIL-12-loaded MBs, concentration, size, and administration route). Future investigations will need to determine the effects of MB number and frequency and pIL-12 administration on the efficacy of our therapeutic strategy in murine models of primary and metastatic melanoma. As previously reported [42, 83, 84], the potential synergy of this strategy with other anti-tumor therapies (*e.g.,* radiotherapy, chemotherapy, and irreversible electroporation) could also be explored under the same *in-vivo* models.

5. Conclusions

In summary, MB-assisted US efficiently delivered pIL-12 *in-vitro* (*i.e.,* suspension of melanoma cells and spheroids) and *in-vivo.* This US modality enhanced the *in-vivo* therapeutic efficacy of IL-12 compared to pIL-12 treatment alone. Nevertheless, further developments and complementary experiments are required to fully potentiate this immunotherapeutic strategy.

In the future, MB-assisted US could serve as a promising approach for *in-vivo* delivery of immunostimulatory molecules, either alone or in combination with other anti-tumor therapies (*e.g.,* chemotherapy, radiotherapy and immunotherapy).

CRediT authorship contribution statement

Edward Oujargir: Writing – review & editing, Writing – Original draft, Software, Methodology, Formal analysis, Data curation, Conceptualization. **Coralie Mousset:** Writing – review & editing, Writing – Original draft, Software, Methodology, Formal analysis, Data curation, Conceptualization. **Marie Roy:** Writing – review & editing, Writing – Original draft, Software, Methodology, Formal analysis, Data curation, Conceptualization. **Yanis Ramdani:** Writing – review & editing, Software, Methodology, Formal analysis, Data curation. **Valérie Schubnel:** Writing – review & editing, Methodology. **Chloé Boisseau:** Writing – review & editing, Methodology. **Sylviane Marouillat:** Writing – review & editing, Methodology. **Rose-Anne Thépault:** Writing – review & editing, Methodology. **Damien Fouan:** Writing – review & editing, Methodology. **Jean-Yves Tartu:** Writing – review & editing, Methodology. **Ayache Bouakaz:** Writing – review & editing. **Sophie Serrière:** Writing – review & editing, Methodology. **Valérie Gouilleux-Gruart:** Writing – review & editing, Validation, Supervision, Funding acquisition, Conceptualization. **Jean-Michel Escoffre:** Writing – review & editing, Writing – original draft, Validation, Supervision, Project administration, Funding acquisition, Conceptualization.

Declaration of competing interest

The authors declare no conflict of interest.

Acknowledgments

The IRIS project (2019-00131873) was supported by the Région Centre-Val de Loire (France) and was approved by the S2E2 cluster. Marie Roy was the recipient of a Ph.D. fellowship from

the Region Centre-Val de Loire. The authors acknowledge Prof. H. Machet, Dr. F. Ossant and Dr. S. Renault (Université de Tours, INSERM, Imaging Brain & Neuropsychiatry iBraiN U1253, 37032, Tours, France) for fruitful discussions and staff members of PST Animalerie (Université de Tours, Tours, France) for the technical assistance. Elsevier Language Editing Services provided English language edition of this manuscript.

Data availability

Data will be made available on request.

References

[1] F. Avry, C. Mousset, E. Oujagir, A. Bouakaz, V. Gouilleux-Gruart, R.A. Thepault, S. Renault, S. Marouillat, L. Machet, J.M. Escoffre, Microbubble-Assisted Ultrasound for Imaging and Therapy of Melanoma Skin Cancer: A Systematic Review, Ultrasound Med Biol, 48 (2022) 2174-2198.

[2] T. Dyba, G. Randi, F. Bray, C. Martos, F. Giusti, N. Nicholson, A. Gavin, M. Flego, L. Neamtiu, N. Dimitrova, R. Negrao Carvalho, J. Ferlay, M. Bettio, The European cancer burden in 2020: Incidence and mortality estimates for 40 countries and 25 major cancers, Eur J Cancer, 157 (2021) 308-347.

[3] C. Karimkhani, A.C. Green, T. Nijsten, M.A. Weinstock, R.P. Dellavalle, M. Naghavi, C. Fitzmaurice, The global burden of melanoma: results from the Global Burden of Disease Study 2015, Br J Dermatol, 177 (2017) 134-140.

[4] J. Dowling, S.P. McGregor, P. Williford, Update on Current Treatment Recommendations for Primary Cutaneous Melanoma, Dermatol Clin, 37 (2019) 397-407.

[5] S. Sarkisian, S. Nair, R. Sharma, Current Clinical Trials in the Treatment of Advanced Melanomas, Surg Clin North Am, 100 (2020) 201-208.

[6] J.K. Schwarze, X. Geeraerts, S. Tuyaerts, B. Neyns, Current "state of the art" on dendritic cell-based cancer vaccines in melanoma, Curr Opin Oncol, 35 (2023) 87-93.

[7] S. Anguille, E.L. Smits, E. Lion, V.F. van Tendeloo, Z.N. Berneman, Clinical use of dendritic cells for cancer therapy, Lancet Oncol, 15 (2014) e257-267.

[8] S. Wilgenhof, A.M.T. Van Nuffel, D. Benteyn, J. Corthals, C. Aerts, C. Heirman, I. Van Riet, A. Bonehill, K. Thielemans, B. Neyns, A phase IB study on intravenous synthetic mRNA electroporated dendritic cell immunotherapy in pretreated advanced melanoma patients, Ann Oncol, 24 (2013) 2686-2693.

[9] G. Trinchieri, Interleukin-12 and the regulation of innate resistance and adaptive immunity, Nat Rev Immunol, 3 (2003) 133-146.

[10] J.A. Gollob, J.W. Mier, K. Veenstra, D.F. McDermott, D. Clancy, M. Clancy, M.B. Atkins, Phase I trial of twice-weekly intravenous interleukin 12 in patients with metastatic renal cell cancer or malignant melanoma: ability to maintain IFN-gamma induction is associated with clinical response, Clin Cancer Res, 6 (2000) 1678-1692.

[11] J.P. Leonard, M.L. Sherman, G.L. Fisher, L.J. Buchanan, G. Larsen, M.B. Atkins, J.A. Sosman, J.P. Dutcher, N.J. Vogelzang, J.L. Ryan, Effects of single-dose interleukin-12 exposure on interleukin-12-associated toxicity and interferon-gamma production, Blood, 90 (1997) 2541-2548.

[12] A.I. Daud, R.C. DeConti, S. Andrews, P. Urbas, A.I. Riker, V.K. Sondak, P.N. Munster, D.M. Sullivan, K.E. Ugen, J.L. Messina, R. Heller, Phase I trial of interleukin-12 plasmid electroporation in patients with metastatic melanoma, J Clin Oncol, 26 (2008) 5896-5903.

[13] S.K. Greaney, A.P. Algazi, K.K. Tsai, K.T. Takamura, L. Chen, C.G. Twitty, L. Zhang, A. Paciorek, R.H. Pierce, M.H. Le, A.I. Daud, L. Fong, Intratumoral Plasmid IL12 Electroporation Therapy in Patients with Advanced Melanoma Induces Systemic and Intratumoral T-cell Responses, Cancer Immunol Res, 8 (2020) 246-254.

[14] U. Kamensek, M. Cemazar, U. Lampreht Tratar, K. Ursic, G. Sersa, Antitumor in situ vaccination effect of TNFalpha and IL-12 plasmid DNA electrotransfer in a murine melanoma model, Cancer Immunol Immunother, 67 (2018) 785-795.

[15] U. Lampreht Tratar, L. Loiacono, M. Cemazar, U. Kamensek, V.M. Fazio, G. Sersa, E. Signori, Gene Electrotransfer of Plasmid-Encoding IL-12 Recruits the M1 Macrophages and Antigen-Presenting Cells Inducing the Eradication of Aggressive B16F10 Murine Melanoma, Mediators Inflamm, 2017 (2017) 5285890.

[16] L. Lambricht, A. Lopes, S. Kos, G. Sersa, V. Preat, G. Vandermeulen, Clinical potential of electroporation for gene therapy and DNA vaccine delivery, Expert Opin Drug Deliv, 13 (2016) 295-310.

[17] V. Malysko-Ptasinske, G. Staigvila, V. Novickij, Invasive and non-invasive electrodes for successful drug and gene delivery in electroporation-based treatments, Front Bioeng Biotechnol, 10 (2022) 1094968.

[18] Y. Endo-Takahashi, Y. Negishi, Gene and oligonucleotide delivery via micro- and nanobubbles by ultrasound exposure, Drug Metab Pharmacokinet, 44 (2022) 100445.

[19] A.P.G. Walsh, H.N. Gordon, K. Peter, X. Wang, Ultrasonic particles: An approach for targeted gene delivery, Adv Drug Deliv Rev, 179 (2021) 113998.

[20] S.R. Sirsi, S.L. Hernandez, L. Zielinski, H. Blomback, A. Koubaa, M. Synder, S. Homma, J.J. Kandel, D.J. Yamashiro, M.A. Borden, Polyplex-microbubble hybrids for ultrasound-guided plasmid DNA delivery to solid tumors, J Control Release, 157 (2012) 224-234.

[21] I. Lentacker, N. Wang, R.E. Vandenbroucke, J. Demeester, S.C. De Smedt, N.N. Sanders, Ultrasound exposure of lipoplex loaded microbubbles facilitates direct cytoplasmic entry of the lipoplexes, Mol Pharm, 6 (2009) 457-467.

[22] J.M. Escoffre, A. Bouakaz, Minireview: Biophysical Mechanisms of Cell Membrane Sonopermeabilization. Knowns and Unknowns, Langmuir, 35 (2019) 10151-10165.

[23] A. Presset, C. Bonneau, S. Kazuyoshi, L. Nadal-Desbarats, T. Mitsuyoshi, A. Bouakaz, N. Kudo, J.M. Escoffre, N. Sasaki, Endothelial Cells, First Target of Drug Delivery Using Microbubble-Assisted Ultrasound, Ultrasound Med Biol, 46 (2020) 1565-1583.

[24] K. Kooiman, S. Roovers, S.A.G. Langeveld, R.T. Kleven, H. Dewitte, M.A. O'Reilly, J.M. Escoffre, A. Bouakaz, M.D. Verweij, K. Hynynen, I. Lentacker, E. Stride, C.K. Holland, Ultrasound-Responsive Cavitation Nuclei for Therapy and Drug Delivery, Ultrasound Med Biol, 46 (2020) 1296-1325.

[25] W. Wang, B. Tayier, L. Guan, F. Yan, Y. Mu, Optimization of the cotransfection of SERCA2a and Cx43 genes for myocardial infarction complications, Life Sci, 331 (2023) 122067.

[26] S. Chen, R.A. Bastarrachea, J.S. Shen, A. Laviada-Nagel, E. Rodriguez-Ayala, E.J. Nava-Gonzalez, P. Huang, R.A. DeFronzo, J.W. Kent, Jr., P.A. Grayburn, Ectopic BAT mUCP-1 overexpression in SKM by delivering a BMP7/PRDM16/PGC-1a gene cocktail or single PRMD16 using non-viral UTMD gene therapy, Gene Ther, 25 (2018) 497-509.

[27] S. Song, M. Noble, S. Sun, L. Chen, A.A. Brayman, C.H. Miao, Efficient microbubble- and ultrasound-mediated plasmid DNA delivery into a specific rat liver lobe via a targeted injection and acoustic exposure using a novel ultrasound system, Mol Pharm, 9 (2012) 2187-2196.

[28] S. Wei, C. Xu, J.J. Rychak, A. Luong, Y. Sun, Z. Yang, M. Li, C. Liu, N. Fu, B. Yang, Short Hairpin RNA Knockdown of Connective Tissue Growth Factor by Ultrasound-Targeted Microbubble Destruction Improves Renal Fibrosis, Ultrasound Med Biol, 42 (2016) 2926-2937.

[29] T. Ilovitsh, Y. Feng, J. Foiret, A. Kheirolomoom, H. Zhang, E.S. Ingham, A. Ilovitsh, S.K. Tumbale, B.Z. Fite, B. Wu, M.N. Raie, N. Zhang, A.J. Kare, M. Chavez, L.S. Qi, G. Pelled, D. Gazit, O. Vermesh, I. Steinberg, S.S. Gambhir, K.W. Ferrara, Low-frequency ultrasound-

mediated cytokine transfection enhances T cell recruitment at local and distant tumor sites, Proc Natl Acad Sci U S A, 117 (2020) 12674-12685.

[30] A.R. Carson, C.F. McTiernan, L. Lavery, A. Hodnick, M. Grata, X. Leng, J. Wang, X. Chen, R.A. Modzelewski, F.S. Villanueva, Gene therapy of carcinoma using ultrasound-targeted microbubble destruction, Ultrasound Med Biol, 37 (2011) 393-402.

[31] K. Ogawa, N. Kato, M. Yoshida, T. Hiu, T. Matsuo, S. Mizukami, D. Omata, R. Suzuki, K. Maruyama, H. Mukai, S. Kawakami, Focused ultrasound/microbubbles-assisted BBB opening enhances LNP-mediated mRNA delivery to brain, J Control Release, 348 (2022) 34-41.

[32] C.Y. Lin, C.H. Tsai, L.Y. Feng, W.Y. Chai, C.J. Lin, C.Y. Huang, K.C. Wei, C.K. Yeh, C.M. Chen, H.L. Liu, Focused ultrasound-induced blood brain-barrier opening enhanced vascular permeability for GDNF delivery in Huntington's disease mouse model, Brain Stimul, 12 (2019) 1143-1150.

[33] C. Zhang, S. Chen, Q. Li, J. Wu, F. Qiu, Z. Chen, Y. Sun, J. Luo, R.A. Bastarrachea, P.A. Grayburn, R.A. DeFronzo, Y. Liu, K. Qian, P. Huang, Ultrasound-Targeted Microbubble Destruction Mediates Gene Transfection for Beta-Cell Regeneration and Glucose Regulation, Small, 17 (2021) e2008177.

[34] X. Xiang, Q. Leng, Y. Tang, L. Wang, J. Huang, Y. Zhang, L. Qiu, Ultrasound-Targeted Microbubble Destruction Delivery of Insulin-Like Growth Factor 1 cDNA and Transforming Growth Factor Beta Short Hairpin RNA Enhances Tendon Regeneration and Inhibits Scar Formation In Vivo, Hum Gene Ther Clin Dev, 29 (2018) 198-213.

[35] Y. Wu, C. Deng, J. Xu, W. Wang, Y. Chen, X. Qin, Q. Lv, M. Xie, Enhanced Local Delivery of microRNA-145a-5P into Mouse Aorta via Ultrasound-Targeted Microbubble Destruction Inhibits Atherosclerotic Plaque Formation, Mol Pharm, 20 (2023) 1086-1095.

[36] C.M. Gorick, A.S. Mathew, W.J. Garrison, E.A. Thim, D.G. Fisher, C.A. Copeland, J. Song, A.L. Klibanov, G.W. Miller, R.J. Price, Sonoselective transfection of cerebral vasculature without blood-brain barrier disruption, Proc Natl Acad Sci U S A, 117 (2020) 5644-5654.

[37] C. Prasad, R. Banerjee, Ultrasound-Triggered Spatiotemporal Delivery of Topotecan and Curcumin as Combination Therapy for Cancer, J Pharmacol Exp Ther, 370 (2019) 876-893.

[38] Y. Hu, S. Xue, T. Long, P. Lyu, X. Zhang, J. Chen, S. Chen, C. Liu, X. Chen, Opto-acoustic synergistic irradiation for vaporization of natural melanin-cored nanodroplets at safe energy levels and efficient sono-chemo-photothermal cancer therapy, Theranostics, 10 (2020) 10448-10465.

[39] O. Zolochevska, X. Xia, B.J. Williams, A. Ramsay, S. Li, M.L. Figueiredo, Sonoporation delivery of interleukin-27 gene therapy efficiently reduces prostate tumor cell growth in vivo, Hum Gene Ther, 22 (2011) 1537-1550.

[40] X. Gao, Y. Nan, Y. Yuan, X. Gong, Y. Sun, H. Zhou, Y. Zong, L. Zhang, M. Yu, Gas-filled ultrasound microbubbles enhance the immunoactivity of the HSP70-MAGEA1 fusion protein against MAGEA1-expressing tumours, Mol Med Rep, 18 (2018) 315-321.

[41] K. Un, S. Kawakami, R. Suzuki, K. Maruyama, F. Yamashita, M. Hashida, Development of an ultrasound-responsive and mannose-modified gene carrier for DNA vaccine therapy, Biomaterials, 31 (2010) 7813-7826.

[42] L. Pasquet, E. Bellard, S. Chabot, B. Markelc, M.P. Rols, J. Teissie, M. Golzio, Pre-clinical investigation of the synergy effect of interleukin-12 gene-electro-transfer during partially irreversible electropermeabilization against melanoma, J Immunother Cancer, 7 (2019) 161.

[43] M. Roy, C. Alix, J. Burlaud-Gaillard, D. Fouan, W. Raoul, A. Bouakaz, E. Blanchard, T. Lecomte, M.C. Viaud-Massuard, N. Sasaki, S. Serriere, J.M. Escoffre, Delivery of Anticancer

Drugs Using Microbubble-Assisted Ultrasound in a 3D Spheroid Model, Mol Pharm, 21 (2024) 831-844.

[44] A. Zeghimi, A. Novell, R.A. Thepault, P. Vourc'h, A. Bouakaz, J.M. Escoffre, Serum influence on in-vitro gene delivery using microbubble-assisted ultrasound, J Drug Target, 22 (2014) 748-760.

[45] N. Zhang, J. Foiret, A. Kheirolomoom, P. Liu, Y. Feng, S. Tumbale, M. Raie, B. Wu, J. Wang, B.Z. Fite, Z. Dai, K.W. Ferrara, Optimization of microbubble-based DNA vaccination with low-frequency ultrasound for enhanced cancer immunotherapy, Adv Ther (Weinh), 4 (2021).

[46] J.M. Escoffre, A. Novell, S. Serriere, T. Lecomte, A. Bouakaz, Irinotecan delivery by microbubble-assisted ultrasound: in vitro validation and a pilot preclinical study, Mol Pharm, 10 (2013) 2667-2675.

[47] D. Bressand, A. Novell, A. Girault, W. Raoul, G. Fromont-Hankard, J.M. Escoffre, T. Lecomte, A. Bouakaz, Enhancing Nab-Paclitaxel Delivery Using Microbubble-Assisted Ultrasound in a Pancreatic Cancer Model, Mol Pharm, 16 (2019) 3814-3822.

[48] H. Akil, J. Rouanet, C. Viallard, S. Besse, P. Auzeloux, J.M. Chezal, E. Miot-Noirault, M. Quintana, F. Degoul, Targeted Radionuclide Therapy Decreases Melanoma Lung Invasion by Modifying Epithelial-Mesenchymal Transition-Like Mechanisms, Transl Oncol, 12 (2019) 1442-1452.

[49] M. Nollet, A.M. Le Guisquet, C. Belzung, Models of depression: unpredictable chronic mild stress in mice, Curr Protoc Pharmacol, Chapter 5 (2013) Unit 5 65.

[50] K.A. Butash, P. Natarajan, A. Young, D.K. Fox, Reexamination of the effect of endotoxin on cell proliferation and transfection efficiency, Biotechniques, 29 (2000) 610-614, 616, 618-619.

[51] E.T. Rietschel, T. Kirikae, F.U. Schade, U. Mamat, G. Schmidt, H. Loppnow, A.J. Ulmer, U. Zahringer, U. Seydel, F. Di Padova, et al., Bacterial endotoxin: molecular relationships of structure to activity and function, FASEB J, 8 (1994) 217-225.

[52] B. Geers, I. Lentacker, A. Alonso, N.N. Sanders, J. Demeester, S. Meairs, S.C. De Smedt, Elucidating the mechanisms behind sonoporation with adeno-associated virus-loaded microbubbles, Mol Pharm, 8 (2011) 2244-2251.

[53] I. De Cock, E. Zagato, K. Braeckmans, Y. Luan, N. de Jong, S.C. De Smedt, I. Lentacker, Ultrasound and microbubble mediated drug delivery: acoustic pressure as determinant for uptake via membrane pores or endocytosis, J Control Release, 197 (2015) 20-28.

[54] B.D. Meijering, L.J. Juffermans, A. van Wamel, R.H. Henning, I.S. Zuhorn, M. Emmer, A.M. Versteilen, W.J. Paulus, W.H. van Gilst, K. Kooiman, N. de Jong, R.J. Musters, L.E. Deelman, O. Kamp, Ultrasound and microbubble-targeted delivery of macromolecules is regulated by induction of endocytosis and pore formation, Circ Res, 104 (2009) 679-687.

[55] M. Derieppe, A. Yudina, M. Lepetit-Coiffe, B.D. de Senneville, C. Bos, C. Moonen, Real-time assessment of ultrasound-mediated drug delivery using fibered confocal fluorescence microscopy, Mol Imaging Biol, 15 (2013) 3-11.

[56] M. Afadzi, S.P. Strand, E.A. Nilssen, S.E. Masoy, T.F. Johansen, R. Hansen, B.A. Angelsen, L.D.C. de, Mechanisms of the ultrasound-mediated intracellular delivery of liposomes and dextrans, IEEE Trans Ultrason Ferroelectr Freq Control, 60 (2013) 21-33.

[57] M. Roy, C. Alix, A. Bouakaz, S. Serriere, J.M. Escoffre, Tumor Spheroids as Model to Design Acoustically Mediated Drug Therapies: A Review, Pharmaceutics, 15 (2023).

[58] B.W. Huang, J.Q. Gao, Application of 3D cultured multicellular spheroid tumor models in tumor-targeted drug delivery system research, J Control Release, 270 (2018) 246-259.

[59] G. Mehta, A.Y. Hsiao, M. Ingram, G.D. Luker, S. Takayama, Opportunities and challenges for use of tumor spheroids as models to test drug delivery and efficacy, J Control Release, 164 (2012) 192-204.

[60] R. Misra, M. Rajic, K. Sathiyamoorthy, R. Karshafian, Ultrasound and microbubbles (USMB) potentiated doxorubicin penetration and distribution in 3D breast tumour spheroids, Joural of Drug Delivery Science and Technology, 61 (2021) 102261.

[61] S. Roovers, J. Deprez, D. Priwitaningrum, G. Lajoinie, N. Rivron, H. Declercq, O. De Wever, E. Stride, S. Le Gac, M. Versluis, J. Prakash, S.C. De Smedt, I. Lentacker, Sonoprinting liposomes on tumor spheroids by microbubbles and ultrasound, J Control Release, 316 (2019) 79-92.

[62] B. Marrero, R. Heller, The use of an in vitro 3D melanoma model to predict in vivo plasmid transfection using electroporation, Biomaterials, 33 (2012) 3036-3046.

[63] L. Wasungu, J.M. Escoffre, A. Valette, J. Teissie, M.P. Rols, A 3D in vitro spheroid model as a way to study the mechanisms of electroporation, Int J Pharm, 379 (2009) 278-284.

[64] M. Azmin, C. Harfield, Z. Ahmad, M. Edirisinghe, E. Stride, How do microbubbles and ultrasound interact? Basic physical, dynamic and engineering principles, Curr Pharm Des, 18 (2012) 2118-2134.

[65] E. Stride, Physical principles of microbubbles for ultrasound imaging and therapy, Front Neurol Neurosci, 36 (2015) 11-22.

[66] J.J. Choi, R.C. Carlisle, C. Coviello, L. Seymour, C.C. Coussios, Non-invasive and real-time passive acoustic mapping of ultrasound-mediated drug delivery, Phys Med Biol, 59 (2014) 4861-4877.

[67] C.A.B. Smith, C.C. Coussios, Spatiotemporal Assessment of the Cellular Safety of Cavitation-Based Therapies by Passive Acoustic Mapping, Ultrasound Med Biol, 46 (2020) 1235-1243.

[68] N. Kopitar-Jerala, The Role of Interferons in Inflammation and Inflammasome Activation, Front Immunol, 8 (2017) 873.

[69] S. Battula, G. Papastoitsis, H.L. Kaufman, K.D. Wittrup, M.M. Schmidt, Intratumoral aluminum hydroxide-anchored IL-12 drives potent antitumor activity by remodeling the tumor microenvironment, JCI Insight, 8 (2023).

[70] A.M. Gocher, C.J. Workman, D.A.A. Vignali, Interferon-gamma: teammate or opponent in the tumour microenvironment?, Nat Rev Immunol, 22 (2022) 158-172.

[71] V. Frenkel, Ultrasound mediated delivery of drugs and genes to solid tumors, Adv Drug Deliv Rev, 60 (2008) 1193-1208.

[72] J.M. Escoffre, A. Zeghimi, A. Novell, A. Bouakaz, In-vivo gene delivery by sonoporation: recent progress and prospects, Curr Gene Ther, 13 (2013) 2-14.

[73] R. Chai, S. Chen, J. Ding, P.A. Grayburn, Efficient, glucose responsive and islet-specific transgene expression by a modified rat insulin promoter, Gene Ther, 16 (2009) 1202-1209.

[74] L. Heller, K. Merkler, J. Westover, Y. Cruz, D. Coppola, K. Benson, A. Daud, R. Heller, Evaluation of toxicity following electrically mediated interleukin-12 gene delivery in a B16 mouse melanoma model, Clin Cancer Res, 12 (2006) 3177-3183.

[75] M.L. Lucas, L. Heller, D. Coppola, R. Heller, IL-12 plasmid delivery by in vivo electroporation for the successful treatment of established subcutaneous B16.F10 melanoma, Mol Ther, 5 (2002) 668-675.

[76] T. Kishida, H. Asada, Y. Itokawa, K. Yasutomi, M. Shin-Ya, S. Gojo, F.D. Cui, Y. Ueda, H. Yamagishi, J. Imanishi, O. Mazda, Electrochemo-gene therapy of cancer: intratumoral delivery of interleukin-12 gene and bleomycin synergistically induced therapeutic immunity and suppressed subcutaneous and metastatic melanomas in mice, Mol Ther, 8 (2003) 738-745.

[77] T. Goto, T. Nishi, O. Kobayashi, T. Tamura, S.B. Dev, H. Takeshima, M. Kochi, J. Kuratsu, T. Sakata, Y. Ushio, Combination electro-gene therapy using herpes virus thymidine

kinase and interleukin-12 expression plasmids is highly efficient against murine carcinomas in vivo, Mol Ther, 10 (2004) 929-937.

[78] E. Cha, A. Daud, Plasmid IL-12 electroporation in melanoma, Hum Vaccin Immunother, 8 (2012) 1734-1738.

[79] H. Li, Y. Zhang, H. Shu, W. Lv, C. Su, F. Nie, Highlights in ultrasound-targeted microbubble destruction-mediated gene/drug delivery strategy for treatment of malignancies, Int J Pharm, 613 (2022) 121412.

[80] R. Abdalkader, S. Kawakami, J. Unga, R. Suzuki, K. Maruyama, F. Yamashita, M. Hashida, Evaluation of the potential of doxorubicin loaded microbubbles as a theranostic modality using a murine tumor model, Acta Biomater, 19 (2015) 112-118.

[81] J. Sitta, F. De Carlo, I. Kirven, J.H. Tackett, P. Penfornis, G.C. Dobbins, M. Barbier, L. Del Valle, C.T. Larsen, E.G. Schutt, R. Li, C.M. Howard, P.P. Claudio, Microbubble-Protected Oncolytic Virotherapy Targeted by Sonoporation Induces Tumor Necrosis and T-Lymphocyte Infiltration in Humanized Mice Bearing Triple-Negative Breast Cancer, Int J Mol Sci, 25 (2024).

[82] K. Yamaguchi, L.B. Feril, Jr., K. Tachibana, A. Takahashi, M. Matsuo, H. Endo, Y. Harada, J. Nakayama, Ultrasound-mediated interferon beta gene transfection inhibits growth of malignant melanoma, Biochem Biophys Res Commun, 411 (2011) 137-142.

[83] A. Sedlar, S. Kranjc, T. Dolinsek, M. Cemazar, A. Coer, G. Sersa, Radiosensitizing effect of intratumoral interleukin-12 gene electrotransfer in murine sarcoma, BMC Cancer, 13 (2013) 38.

[84] U. Kamensek, G. Sersa, M. Cemazar, Evaluation of p21 promoter for interleukin 12 radiation induced transcriptional targeting in a mouse tumor model, Mol Cancer, 12 (2013) 136.